8-10-2021

Evaluating Prediction Models of Creep and Drying Shrinkage of Self-Consolidating Concrete Containing Supplementary Cementitious Materials/Fillers

Micheal Asaad

George Morcous

applied sciences

MDPI

Article

Evaluating Prediction Models of Creep and Drying Shrinkage of Self-Consolidating Concrete Containing Supplementary Cementitious Materials/Fillers

Micheal Asaad and George Morcous *

Durham School of Architectural Engineering and Construction, College of Engineering, University of Nebraska—Lincoln (UNL), 1110 South 67th Street, Omaha, NE 68182-0816, USA; Micheal.Asaad@kiewit.com
* Correspondence: gmorcous2@unl.edu

Abstract: Supplementary cementitious materials (SCMs) and fillers play an important role in enhancing the mechanical properties and durability of concrete. SCMs and fillers are commonly used in self-consolidating concrete (SCC) mixtures to also enhance their rheological properties. However, these additives could have significant effects on the viscoelastic properties of concrete. Existing models for predicting creep and drying shrinkage of concrete do not consider the effect of SCM/filler on the predicted values. This study evaluates existing creep and drying shrinkage models, including AASHTO LRFD, ACI209, CEB-FIP MC90-99, B3, and GL2000, for SCC mixtures with different SCMs/fillers. Forty SCC mixtures were proportioned for different cast-in-place bridge components and tested for drying shrinkage. A set of eight SCC mixtures with the highest paste content was tested for creep. Shrinkage and creep test results indicated that AASHTO LRFD provides better creep prediction than the other models for SCC with different SCMs/fillers. Although all models underestimate drying shrinkage of SCC with different SCMs/fillers, the GL2000, CEB-FIP MC90-99, and ACI 209 models provide better prediction than AASHTO LRFD and B3 models. Additionally, SCC mixtures with limestone powder filler exhibited the highest creep, while those with class C fly ash exhibited the highest drying shrinkage.

Keywords: self-consolidating concrete; viscoelastic properties; creep; drying shrinkage; supplementary cementitious materials; fillers; prediction models

Citation: Asaad, M.; Morcous, G. Evaluating Prediction Models of Creep and Drying Shrinkage of Self-Consolidating Concrete Containing Supplementary Cementitious Materials/Fillers. *Appl. Sci.* **2021**, *11*, 7345. https://doi.org/10.3390/app11167345

Academic Editor: Young Hoon Kim

Received: 15 July 2021
Accepted: 3 August 2021
Published: 10 August 2021

1. Introduction

Self-consolidating concrete (SCC) is highly flowable, non-segregating concrete that can spread into place, fill the formwork, and encapsulate the reinforcement without any mechanical consolidation [1]. To enhance the stability of SCC, supplementary cementitious materials (SCMs)/fillers are used to improve the viscosity and quality of paste in addition to mechanical and durability properties. The binder composition of SCC, in addition to many other factors, affects its viscoelastic properties, primarily shrinkage and creep. However, existing creep and drying shrinkage prediction models do not account for the effect of SCM/filler type on the predicted values for SCC. Therefore, the objective of this study is to evaluate creep and drying shrinkage prediction models including AASHTO LRFD [2], ACI 209 [3,4], CEB-FIP MC90-99 [5], B3 [6], and GL2000 [7] for SCC mixtures containing different types of SCM/filler.

To achieve this objective, a literature review was conducted to determine the different prediction models for shrinkage and creep of SCC as well as the effect of SCMs/fillers on its viscoelastic properties. Fresh, early-age, and hardened concrete properties were evaluated in a laboratory investigation of forty SCC mixtures proportioned using: two types of coarse aggregate—crushed limestone and natural gravel; three nominal maximum sizes of aggregate (NMSA)—$\frac{3}{4}$, $\frac{1}{2}$, and $^{3}/_{8}$ in.; three SCMs and one filler—25% Class F fly ash, 25% Class C fly ash, 30% ground granulated blast-furnace slag (GGBFS), and 20% Class

F fly ash +15% limestone powder (LSP); and two levels of slump flow—low (22–26 in.) and high (26–30 in.). All SCC mixtures were air entrained and contained Portland cement Type I/II, which is the common practice in cast-in-place bridge construction. The laboratory tests were conducted according to AASHTO or ASTM methods. Measured properties of SCC mixtures were compared to predicted values using the five prediction models listed earlier.

1.1. Creep Models

Many researchers reported diverse conclusions regarding the viscoelastic properties of SCC due to the variations in the used mixture proportions and testing conditions. Leemann et al. [8] reported that the higher the paste volume of SCC, the higher the creep strain. Turcry et al. [9] reported no difference in creep strain between conventional vibrated concrete (CVC) and SCC, which have similar compressive strength. Heirman et al. [10] reported that the use of LSP as a filler increases creep strain as a result of the slow gain of concrete compressive strength. Kavanaugh [11] reported that the use of low water-cementitious material ratio (w/cm) decreases permeability of SCC mixtures and provides less creep compliance than CVC at all ages.

Kim et al. [12] reported that the AASHTO LRFD (2007) [13] predicts the creep compliance with the highest accuracy among all models. The AASHTO LRFD (2004) [14], ACI 209 and CEB-FIP MC90-99 models provide fairly good predictions of the creep compliance for both CVC and SCC mixtures, while the CEB-FIP MC90, B3, and GL2000 models overestimate the creep compliance. Khayat and Mitchell [15] reported that the CEB-FIP MC90-99 model provides the highest accuracy among all models for predicting creep strains. The ACI 209, AASHTO LRFD (2004), and AASHTO LRFD (2007) models underestimate creep strains at most loading ages, while the GL2000 model overestimates the creep strains. Kavanaugh [12] reported that the AASHTO LRFD (2007) underestimates the creep strain of early-age concrete and overestimates the creep strain of later-age concrete. The CEB-FIP MC90 model accurately predicts creep for both CVC and SCC. The GL 2000 model overestimates the creep strain of both the CVC and SCC mixtures. The ACI 209 model does not accurately predict the creep strain of high-strength concrete mixtures. Heirman et al. [10] reported that the CEB-FIP MC90 model can be used for predicting the creep of SCC mixtures with LSP. Landsberger and Fernandez-Gomez [16] reported that the CEB-FIP MC90, ACI 209, B3 and GL2000 models underestimate the creep strain and the ACI 209 model predicts the creep strain with the least dispersion. Naito et al. [17] reported that the ACI 209 model underestimates the creep coefficient for both CVC and SCC but dramatically for the latter one.

1.2. Drying Shrinkage Models

Higher drying (free) shrinkage of SCC is expected due to the denser matrix of the system, which leads to small capillary voids and allows faster removal of water than large voids [18]. Additionally, using finer cement leads to higher drying shrinkage due to the pore refinement [19]. On the other hand, using fly ash and GGBFS reduces the drying shrinkage of SCC, while the silica fume increases the drying shrinkage when used in binary blends [20,21]. The shrinkage of high early-strength SCC is similar to or less than that of CVC and there is no significant effect of fine aggregate ratio [22]. Naito et al. [17] presented higher viscoelastic properties of SCC than CVC due to the higher fine aggregate volume in SCC.

Khayat and Mitchell [15] reported that all models underestimate the drying shrinkage of SCC; however, the CEB-FIP MC90 model provides the best prediction of drying shrinkage of SCC as it considers the effect of cement type. Landsberger and Fernandez-Gomez [16] reported that the ACI 209R model provides the best prediction of drying shrinkage of SCC, while the CEB-FIP MC90 and GL2000 models substantially underestimate it. Schindler et al. [22] reported that the ACI 209R model accurately predicts the shrinkage of SCC at later ages (56 and 112 days), while the AASHTO LRFD (2004) model underestimates SCC shrinkage at early ages (7 and 14 days) and overestimates it at later

ages (56 and 112 days). Naito et al. [17] reported that the ACI 209 model overestimates the drying shrinkage for both SCC and high early strength concrete.

2. Experimental Investigation

2.1. Material Properties

Table 1 and Figure 1 show, respectively, the chemical composition and particle size distribution of the cement type I/II, SCMs (class F fly ash, class C fly ash, GGBFS), and filler (limestone powder) used in the experimental investigation. Two different types of coarse aggregate, crushed limestone and gravel, were used in this investigation. The two types were combined with fine aggregate (natural sand) using three different fine-to-coarse aggregate ratios of 0.45, 0.47, and 0.50. All physical properties and particle size distribution of fine and coarse aggregates are shown in Table 2 and Figure 2, respectively, and the combined aggregate gradations used in SCC mixtures are listed in Table 3. Chemical admixtures included polycarboxylate type high range water reducing admixture (HRWRA) that meets the requirements of ASTM C494 type F admixture; viscosity-modifying admixture (VMA) that meets the requirement of ASTM C494 type S admixture; and air-entraining admixture (AEA) that meets the requirements of ASTM C 260. All materials used in this investigation were obtained from suppliers in the Midwest states of Nebraska, Iowa, and Minnesota.

Table 1. Chemical composition of cement, SCMs, and filler.

Chemical Component	Type I/II Cement (%)	Class C Fly Ash (%)	Class F Fly Ash (%)	Limestone Powder (%)	GGBFS (%)
SiO_2	20.10	42.46	50.87	1.56	31.63
Al_2O_3	4.44	19.46	20.17	-	11.30
Fe_2O_3	3.09	5.51	5.27	0.48	0.34
SO_3	3.18	1.20	0.61	1.77	3.30
CaO	62.94	21.54	15.78	52.77	41.31
MgO	2.88	4.67	3.19	0.48	10.77
Na_2O	0.10	1.42	0.69	0.03	0.19
K_2O	0.61	0.68	1.09	0.09	0.36
P_2O_5	0.06	0.84	0.44	-	0.02
TiO_2	0.24	1.48	1.29	-	0.56
SrO	0.09	0.32	0.35	-	0.04
BaO	-	0.67	0.35	-	-
LOI	2.22	0.19	0.07	42.50	-

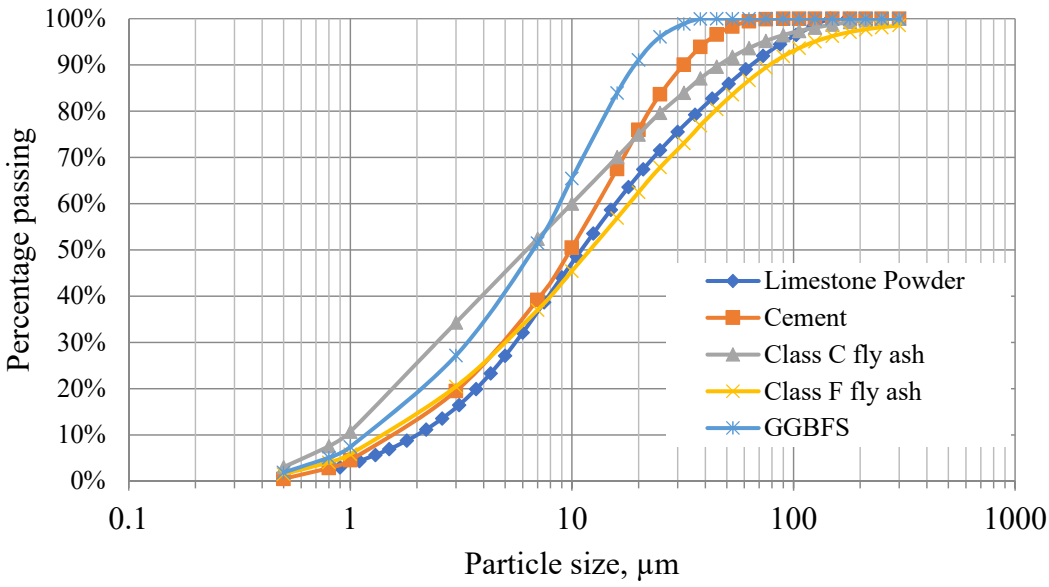

Figure 1. Particle size distribution of cement, SCMs, and filler (25 mm = 1 in.).

Table 2. Physical properties of aggregates (25 mm = 1 in.).

PROPERTY	Limestone NMSA			Gravel NMSA			River Sand
	19.0 mm	12.5 mm	9.5 mm	19.0 mm	12.5 mm	9.5 mm	
Specific Gravity (SSD)	2.66	2.66	2.66	2.74	2.68	2.69	2.62
Absorption %	1.3	1.3	1.3	1.1	1.4	1.4	0.5
S/A Ratio	0.45	0.47	0.50	0.45	0.47	0.50	N/A
Combined DRUW (kg/m^3)	1874	1890	1890	2035	1986	1970	N/A
Voids, %	29.0	28.4	28.4	23.7	25.9	27.0	N/A

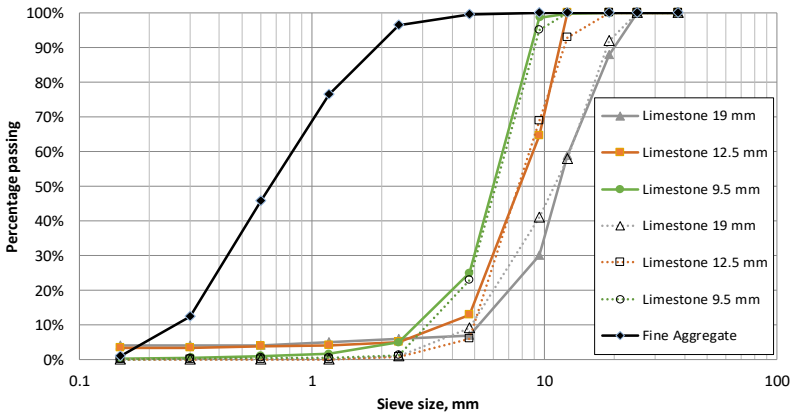

Figure 2. Particle size distribution of fine and coarse aggregates (25 mm = 1 in.).

Table 3. Combined aggregate gradations (25 mm = 1 in.).

Sieve Size		Sand and Limestone			Sand and Gravel		
		S/A Ratio			S/A Ratio		
No.	mm	0.45	0.47	0.50	0.45	0.47	0.50
		19.0 mm	12.5 mm	9.5 mm	19.0 mm	12.5 mm	9.5 mm
1″	25.4	100.0	100.0	100.0	100.0	100.0	100.0
3/4″	19	93.4	100.0	100.0	97.8	100.0	100.0
1/2″	12.5	77.5	100.0	100.0	79.7	95.8	99.9
3/8″	9.5	61.5	81.3	99.4	67.6	82.5	97.0
#4	4.75	48.7	53.7	62.4	48.3	48.4	60.9
#8	2.36	46.7	48.0	50.8	43.9	45.4	48.8
#16	1.18	37.2	38.2	39.2	34.6	36.1	38.5
#30	0.6	22.9	23.6	23.5	20.8	21.7	23.1
#50	0.3	7.8	7.7	6.6	5.7	6.0	6.4
#100	0.15	2.6	2.2	0.6	0.5	0.5	0.5
#200	0	-	-	-	-	-	-

2.2. Mixture Proportioning

Two groups of SCC mixtures were proportioned: one with crushed limestone coarse aggregate (LS), and the other with gravel (G). Each group had 20 mixtures as follows: 5 mixtures had 25% powder replacement with class C fly ash (C), 5 mixtures had 25% powder replacement with class F fly ash (F), 5 mixtures had 30% powder replacement with GGBFS (S), and 5 mixtures had 35% powder replacement with class F fly ash (20%) and limestone powder (15%) (FLP). Each group had NMSA of 19 mm ($\frac{3}{4}$ in.), 12.5 mm ($\frac{1}{2}$ in.), and 9.5 mm ($^3/_8$ in.) with two levels of filling ability: high flow (HF), where slump flow is less than 750 mm (30 in.) but greater than or equal to 650 mm (26 in.); and low flow (LF), where slump flow is less than 650 mm (26 in.) but greater than or equal to 550 mm (22 in.). Table 4a,b present the proportions of the forty SCC mixtures containing limestone and gravel aggregate, respectively.

Table 4. (**a**) Proportions for SCC mixtures containing limestone aggregate (25 mm = 1 in.; 1000 kg/m^3 = 1686 lb/cy; 65 mL/100 kg = 1 oz/cwt). (**b**) Proportions for SCC mixtures containing gravel aggregate (25 mm = 1 in.; 1000 kg/m^3 = 1686 lb/cy; 65 mL/100 kg = 1 oz/cwt).

(**a**)

Coarse Aggregate	**Crushed Limestone (LS)**																			
SCMs and Fillers	**25% Class C Fly Ash (C)**					**25% Class F Fly Ash (F)**					**30% GGBFS (S)**					**20% Class F Fly Ash + 15% LSP (FLP)**				
Filling Ability	**Low Flow (LF)**		**High Flow (HF)**			**Low Flow (LF)**		**High Flow (HF)**			**Low Flow (LF)**		**High Flow (HF)**			**Low Flow (LF)**		**High Flow (HF)**		
NMAS	**19 mm**	**12.5 mm**	**19 mm**	**12.5 mm**	**9.5 mm**	**19 mm**	**12.5 mm**	**19 mm**	**12.5 mm**	**9.5 mm**	**19 mm**	**12.5 mm**	**19 mm**	**12.5 mm**	**9.5 mm**	**19 mm**	**12.5 mm**	**19 mm**	**12.5 mm**	**9.5 mm**
Cement I/II, kg/m^3	315	317	337	339	348	315	317	337	339	348	309	311	320	322	331	271	273	289	292	299
SCM, kg/m^3	105	106	112	113	116	105	106	112	113	116	132	133	137	138	142	83	84	89	90	92
Filler, kg/m^3	0	0	0	0	0	0	0	0	0	0	0	0	0	0	0	62	63	67	67	69
Coarse Agg., kg/m^3	915	867	900	853	792	915	867	900	853	792	915	867	908	860	798	915	867	900	853	792
Natural Sand, kg/m^3	749	769	737	757	792	749	769	737	757	792	749	769	743	763	798	749	769	737	757	792
Water, kg/m^3	166	175	166	175	181	166	175	166	175	181	166	175	166	175	181	166	175	166	175	181
HRWRA, mL/100 kg	780	910	780	1040	845	390	260	520	520	845	780	650	1170	1040	975	715	585	780	780	975
VMA, mL/100 kg	0	0	390	0	0	195	0	195	390	0	0	0	195	195	0	0	0	195	390	0
AEA, mL/100 kg	98	98	98	98	98	98	98	98	98	98	98	98	98	98	98	98	98	98	98	98
Paste Volume %	37.0	38.0	38.0	39.0	40.0	37.0	38.0	38.0	39.0	40.0	37.0	38.0	37.5	38.5	39.5	37.0	38.0	38.0	39.0	40.0

(**b**)

Coarse Aggregate	**Gravel (G)**																			
SCMs and Fillers	**25% Class C Fly Ash (C)**					**25% Class F Fly Ash (F)**					**30% GGBFS (S)**					**20% Class F Fly Ash + 15% LSP (FLP)**				
Filling Ability	**Low Flow (LF)**		**High Flow (HF)**			**Low Flow (LF)**		**High Flow (HF)**			**Low Flow (LF)**		**High Flow (HF)**			**Low Flow (LF)**		**High Flow (HF)**		
NMSA	**19 mm**	**12.5 mm**	**19 mm**	**12.5 mm**	**9.5 mm**	**19 mm**	**12.5 mm**	**19 mm**	**12.5 mm**	**9.5 mm**	**19 mm**	**12.5 mm**	**19 mm**	**12.5 mm**	**9.5 mm**	**19 mm**	**12.5 mm**	**19 mm**	**12.5 mm**	**9.5 mm**
Cement I/II, kg/m^3	293	295	337	339	348	293	295	337	339	348	287	290	320	344	331	261	263	289	292	299
SCM, kg/m^3	98	98	112	113	116	98	98	112	113	116	123	124	137	147	142	80	81	89	90	92
Filler, kg/m^3	0	0	0	0	0	0	0	0	0	0	0	0	0	0	0	60	61	67	67	69
Coarse Agg., kg/m^3	937	888	908	860	797	937	888	908	860	797	937	888	915	853	804	930	881	908	860	797
Natural Sand, kg/m^3	767	788	743	763	797	767	788	743	763	797	767	788	749	757	804	761	782	743	763	797
Water, kg/m^3	166	175	166	175	181	166	175	166	175	181	166	175	166	175	181	166	175	166	175	181
HRWRA, mL/100 kg	325	98	585	325	520	455	260	455	325	358	390	325	650	455	488	195	195	390	488	390
VMA, mL/100 kg	0	0	195	0	195	0	0	130	195	195	0	0	195	0	0	0	0	130	195	0
AEA, mL/100 kg	98	98	98	98	98	98	98	98	98	98	98	98	98	98	98	98	98	98	98	98
Paste Volume %	36.0	37.0	38.0	39.0	40.0	36.0	37.0	38.0	39.0	40.0	36.0	37.0	37.5	39.5	39.5	36.5	37.5	38.0	39.0	40.0

2.3. Workability Testing

All SCC mixtures were proportioned to achieve acceptable levels of filling ability, passing ability and stability (static and dynamic). These properties, except dynamic stability, were assessed using standard test methods to assure the quality of the fresh SCC. Filling ability was evaluated using the slump flow test of the inverted cone in accordance with ASTM C1611. As an indication of the viscosity of the mixtures, the time of reaching 500 mm spread diameter (T_{50}) was also measured. The passing ability of fresh SCC was determined using the J-ring test method according to ASTM C1621. Two parameters were used to describe the passing ability of fresh SCC: (1) the difference between average slump flows (ΔD) in restrained (with J-ring) and unrestrained conditions (without J-ring); (2) the difference between the height of concrete patty in the middle of the J-ring, and the average height of the patty at four points around the perimeter of J-ring (ΔH) according to AASHTO T 345. The higher the ΔD and ΔH, the higher the probability of blockage when SCC flows around reinforcing bars. The filling capacity of fresh SCC was determined using the caisson test method and according to AASHTO T 349. The measured filling capacity represents the ability of fresh SCC to fill the forms while passing through cross bars. The static stability of SCC was determined using the four standardized test methods: penetration test according to ASTM C1712, column test according to ASTM C1610, visual stability index (VSI) according to ASTM C1611, and hardened visual stability index (HVSI) according to AASHTO PP 58. Dynamic stability was evaluated using the flow-through test according to Lange et al. [23], as no standard test method is available for this property. Additionally, mortar and concrete rheometers were used to characterize the rheological properties of SCC mixtures. Dynamic yield stress and plastic viscosity (i.e., Bingham model parameters) were determined using Brookfield mortar rheometer according to ASTM C1749, while yield torque and slope were determined using IBB concrete rheometer according to Hu and Wang [24].

2.4. Creep Testing

Creep strain was measured according to ASTM C512 for only eight SCC mixtures due to the availability of testing frame and length of test duration. SCC mixtures containing limestone and gravel aggregates with NMSA of 9.5 mm ($^3/_8$ in.) were chosen because they have the highest paste volume and, consequently, are expected to have the highest creep strains. A set of two 150 × 300 mm (6 × 12 in.) cylinders was obtained from each mixture and loaded to 40 percent of their 28-day average compressive strength after 28 days from the casting date, and another set of two similar cylinders was unloaded and monitored for deformations due to shrinkage and temperature effects as shown in Figure 3. The average temperature and humidity of the room are 20 degrees Celsius and 38%, respectively.

All cylinders were instrumented using three pairs of detachable mechanical (DEMEC) gauges distributed around the cylinders to measure the longitudinal deformations over 8 in. distance using a dial gauge. The deformations for both sets were recorded every day for a week, then every 7 days for a month, and then every 30 days up to 360 days after time of loading for all mixtures except for mixture with gravel and class C fly ash (G-C) up to 270 due to erroneous readings after 270 days. Average creep strains were calculated by subtracting the average deformation of the unloaded cylinders from those of the loaded cylinders to eliminate shrinkage strain. Additionally, measurements from the three pairs of gauges were compared to check the uniformity of loading. Table 5 lists the five creep prediction models used to estimate the creep coefficient of SCC mixtures. Descriptions of all the model parameters are presented in the notations section at the end of the paper.

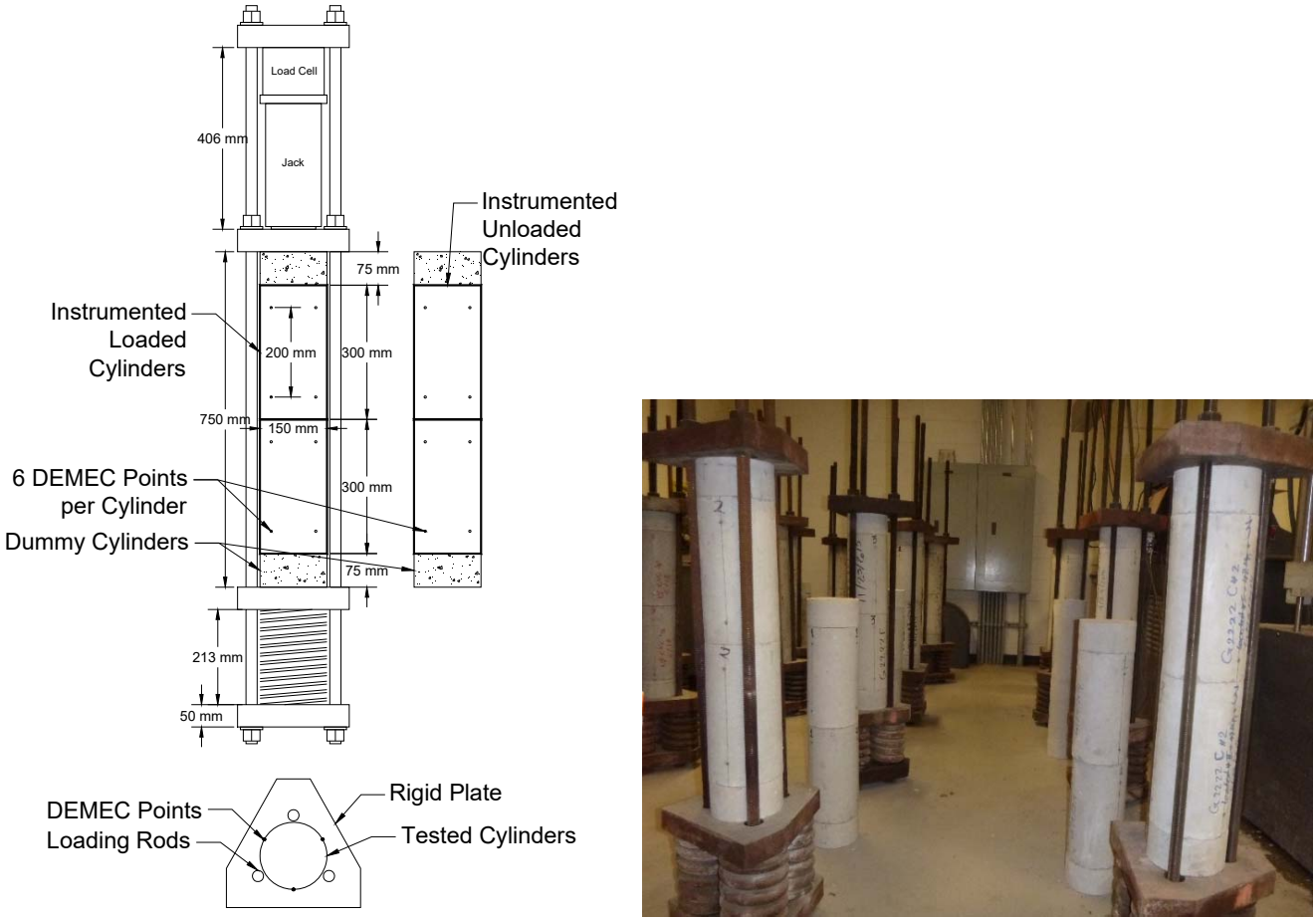

Figure 3. Creep test setup and specimen dimensions (25 mm = 1 in.).

Table 5. Creep coefficient prediction models.

Model Name	Creep Coefficient Prediction Equation, $\phi(t,t_o)$
AASHTO LRFD [2]	$1.9\, k_s\, k_{hc}\, k_f\, k_{td}\, t_i^{-0.118}$
ACI 209 [3,4]	$\frac{(t-to)^{\Psi}}{d+(t-to)^{\Psi}} \cdot \phi_u$
CEB-FIP MC90-99 [5]	$\phi_o\, \beta_c(t-t_o)$
B3 [6]	$E_{cmto}(q_1 + C_o(t,t_o) + C_d(t,t_o,t_c)) - 1$
GL 2000 [7]	$\Phi(t_c)[2\, \frac{(t-to)^{0.3}}{(t-to)^{0.3}+14} + \left(\frac{7}{t_o}\right)^{0.5} (\frac{(t-to)}{(t-to)+7})^{0.5} + 2.5(1-1.086h^2)(\frac{t-t_o}{t-t_o+0.12\left(\frac{v}{s}\right)^2})^{0.5}]$

2.5. Drying Shrinkage Testing

The drying shrinkage was measured in accordance with ASTM C157 for all forty SCC mixtures as shown in Figure 4. Three concrete prisms that are 76 × 76 × 286 mm 3 × 3 × 11 $\frac{1}{4}$ in.) from each mixture were moist cured for 7 days and maintained at 50% ± 4% relative humidity and 23 ± 2 °C temperature until 56 days. The readings were made at 3, 7, 14, 28, and 56 days after the curing period. Table 6 lists the five shrinkage prediction models used to estimate the drying shrinkage strains of SCC mixtures and compared then with the measured values. Descriptions of all the model parameters are presented in the notations section at the end of the paper.

Figure 4. Drying shrinkage specimens.

Table 6. Drying shrinkage strain prediction models.

Model Name	Drying Shrinkage Strain Prediction Equation, $\varepsilon(t,t_c)$
AASHTO LRFD [2]	$k_s\ k_{hs}\ k_f\ k_{td}\ 0.48 \times 10^{-3}$
ACI 209 [3,4]	$\frac{(t-tc)^{\alpha}}{f+(t-tc)^{\alpha}} \cdot \varepsilon_{shu}$
CEB-FIP MC90-99 [5]	$\varepsilon_{cso}\ \beta_s(t-t_c)$
B3 [6]	$\varepsilon_{sh\infty} k_h\ S(t-t_c)$
GL 2000 [7]	$\varepsilon_{shu}\ \beta(h)\ \beta(t-t_c)$

3. Results and Discussion

3.1. Workability Properties

Table 7 summarizes the workability properties of all SCC mixtures considered in this investigation. SCC mixtures designed for low filling ability had slump flow between 550 and 650 mm (22 and 26 in.), while those designed for high filling ability had slump flow between 650 and 750 mm (26 and 30 mm). T50 was found to be ≤2 s for all mixtures, which indicates the low viscosity of the tested mixtures. Most mixtures had satisfactory passing ability as ΔD is ≤50 mm (2 in.) and ΔH ≤ 15 mm (0.6 in.). Only a few mixtures, mostly with NMSA = 19 mm ($^3/_4$ in.), presented higher probability of blockage. All mixtures had adequate filling capacity more than 70%. Most SCC mixtures had adequate static stability as the penetration values (average of two measurements) were less than 25 mm (1 in.) and column segregation percentage was less than 15%. A few mixtures, mostly with NMSA = 19 mm ($^3/_4$ in.), had lower static stability as penetration was equal to 25 mm (1 in.) and column segregation percentage was between 15% and 20%, which might be acceptable for some cast-in-place components. The VSI and HVSI for all SCC mixtures were either 0 or 1, which indicated adequate stability. It should be noted that VSI and HVSI are qualitative test methods that depend on the operator judgment; however, the guidelines presented in test standards were followed to minimize the subjectivity of the assessment. Dynamic stability was measured using the flow-through method for only SCC mixtures with high slump flow. Results indicated that most mixtures had exhibited either high dynamic stability (segregation ≤20%) or moderate dynamic stability (segregation ≤30%). Most SCC mixtures with high slump flow and $\frac{3}{4}$ in. NMSA had shown poor dynamic stability, making them inappropriate for long or deep components.

Table 7. Workability properties of SCC mixtures (25 mm = 1 in.; 1000 pa = 0.145 psi; 1 N-m = 8.85 lb-in.).

Coarse Aggregate Type	NMSA (mm)	ID	Slump Flow			J-Ring		Caisson	Penetration	Column Technique	Long Trough	Static Stability	Dynamic Yield Stress	Plastic Viscosity	Yield Torque	Slope
			D_{av} (mm)	T_{50} (s)	VSI	ΔD (mm)	ΔH (mm)	FC (%)	P_d (mm)	Seg. (%)	Seg. (%)	HVSI	Pa	Pa-s	N-m	N-m-s
Limestone	19	C_LF	654	1.9	0	102	14	75.5%	4	5.2%	7.2%	1	78.7	1.07	1.11	2.95
	19	F_LF	667	1.2	1	114	14	79.0%	2	13.2%	N/A	0	61.95	0.93	1.01	2.94
	19	S_LF	578	1.7	0	83	16	80.6%	6	4.2%	N/A	1	53.54	1.17	1.14	3.34
	19	FLP_LF	572	1.9	0	38	16	70.2%	3	2.1%	N/A	0	49.87	0.83	1.02	2.87
	19	C_HF	635	2.0	0	19	6	75.5%	3	0.4%	32.0%	1	37.87	1.73	0.78	3.89
	19	F_HF	686	1.2	1	64	14	86.1%	6	3.9%	35.7%	1	26.8	0.87	0.61	3.32
	19	S_HF	686	2.0	1	13	13	78.3%	10	10.8%	10.2%	0	10.73	1.95	0.54	4.78
	19	FLP_HF	660	2.0	1	19	11	81.4%	6	13.9%	24.3%	1	53.11	1.08	0.88	3.83
	12.5	C_LF	629	2.0	1	32	5	80.8%	3	2.0%	N/A	0	45.44	0.97	1.03	3.29
	12.5	F_LF	641	2.0	0	22	4	91.5%	6	10.1%	N/A	0	51.56	1.07	0.84	3.13
	12.5	S_LF	572	2.0	0	13	14	81.7%	6	0.0%	N/A	1	47.08	1.39	1	3.96
	12.5	FLP_LF	660	2.0	1	6	10	91.2%	6	4.9%	N/A	0	40.73	0.89	0.84	2.48
	12.5	C_HF	660	2.0	0	6	3	71.4%	4	2.1%	5.21%	1	29.29	0.71	0.65	2.03
	12.5	F_HF	673	2.0	0	38	11	79.6%	5	5.2%	39.9%	1	39.5	1.03	0.8	3.08
	12.5	S_HF	775	2.0	0	25	0	95.8%	3	5.50%	35.6%	1	14.77	1.08	0.68	3.3
	12.5	FLP_HF	692	2.0	1	6	3	94.2%	13	8.1%	23.4%	1	30.88	0.82	0.86	3.11
	9.5	C_HF	679	2.0	0	13	13	83.3%	4	3.4%	25.5%	0	24.61	1	0.87	3.35
	9.5	F_HF	737	2.0	1	13	6	91.4%	2	0.0%	11.9%	1	27.6	0.88	0.87	2.47
	9.5	S_HF	667	2.7	0	0	8	89.5%	14	3.0%	18.3%	0	20.29	1.73	0.78	4.69
	9.5	FLP_HF	705	1.7	0	6	N/A	93.7%	6	3.8%	N/A	0	33.3	1.09	0.7	2.64
Gravel	19	C_LF	622	1.6	1	51	13	86.2%	3	12.7%	N/A	1	87.63	1.89	3.79	1.28
	19	F_LF	622	1.2	1	32	6	90.2%	6	9.5%	N/A	1	50.72	0.79	2.71	1.04
	19	S_LF	597	1.9	0	19	16	82.8%	3	9.8%	N/A	0	45.16	1.42	3.24	1.5
	19	FLP_LF	565	1.4	0	6	19	73.2%	0	17.4%	N/A	1	43.5	0.64	2.51	1.17

Table 7. *Cont.*

Coarse Aggregate Type	NMSA (mm)	ID	Slump Flow			J-Ring		Caisson	Penetration	Column Technique	Long Trough	Static Stability	Dynamic Yield Stress	Plastic Viscosity	Yield Torque	Slope
			D_{av} (mm)	T_{50} (s)	VSI	ΔD (mm)	ΔH (mm)	FC (%)	P_d (mm)	Seg. (%)	Seg. (%)	HVSI	Pa	Pa-s	N-m	N-m-s
Gravel	19	C_HF	692	1.3	1	19	6	91.8%	13	3.7%	19.3%	1	38.63	1.23	3.01	0.98
	19	F_HF	724	1.2	1	13	0	96.2%	19	18.9%	45.0%	1	18.58	0.82	2.63	0.76
	19	S_HF	705	2.3	1	19	6	95.1%	25	18.4%	45.5%	1	13.5	1.98	2.15	1.19
	19	FLP_HF	711	1.6	1	32	6	94.1%	16	19.3%	37.6%	1	12.83	0.57	2.11	0.65
	12.5	C_LF	635	1.0	0	25	3	87.6%	6	1.0%	N/A	1	55.2	0.77	2.68	1.18
	12.5	F_LF	565	1.4	0	70	19	71.2%	0	4.8%	N/A	0	44.47	0.62	2.32	0.99
	12.5	S_LF	591	1.8	0	0	13	82.3%	6	2.7%	6.9%	1	31.1	1.15	2.72	1.06
	12.5	FLP_LF	597	1.0	0	32	6	89.6%	3	5.1%	N/A	0	25.92	0.59	1.91	0.72
	12.5	C_HF	660	1.5	0	25	6	94.4%	13	4.1%	25.5%	0	25.98	0.52	2.17	0.84
	12.5	F_HF	660	1.1	0	13	6	88.4%	6	1.4%	4.3%	0	8.36	0.4	1.49	0.79
	12.5	S_HF	686	2.3	0	0	13	92.4%	6	12.7%	16.8%	0	1.39	0.68	1.38	0.58
	12.5	FLP_HF	699	0.9	1	13	6	93.9%	13	9.0%	20.9%	1	15.77	0.46	1.56	0.87
	9.5	C_HF	699	1.4	0	38	6	93.9%	16	5.1%	15.6%	0	18.93	0.88	2.61	0.56
	9.5	F_HF	730	1.3	1	19	6	93.5%	25	11.4%	15.8%	0	9.75	0.74	1.44	0.68
	9.5	S_HF	667	1.8	1	13	6	89.5%	6	18.1%	5.0%	0	0	0.53	1.49	0.53
	9.5	FLP_HF	686	1.1	0	19	0	95.2%	16	12.4%	2.4%	0	11.36	0.69	2.03	0.45

Two parameters were measured to evaluate the rheology of SCC mixtures: (1) yield torque, which represents yield stress; (2) slope of the rheological model, which indicates plastic viscosity. The effects of different types of SCM/filler on the rheological properties were not significant. However, the SCC mixtures with larger coarse aggregate (NMSA = 19 mm) represented higher yield torque compared to those with smaller aggregate (NMSA = 9.5 mm). Additionally, SCC mixtures containing gravel aggregate had higher yield torque and lower viscosity than SCC mixtures containing limestone aggregate.

3.2. Creep Coefficient

Figure 5 plots the measured creep strain for tested SCC mixtures, while Figure 6 plots the creep coefficient curves for these mixtures. Creep coefficient represents the ratio of the creep strain to elastic strain at a stress level of 40% of the average 28-day compressive strength. The first readings were recorded at the first day after loading. Statistical analysis was conducted to show whether there was a significant difference between predicted and measured creep coefficient ratios when different types of SCMs/fillers were used. Table 8 shows the results in terms of average and variance of predicted-to-measured creep coefficient ratio. Comparing the results of all models indicates that ACI 209 and AASHTO LRFD models slightly underestimate the creep coefficient, while CEB-FIP MC90-99 and GL2000 models significantly overestimate the creep coefficient.

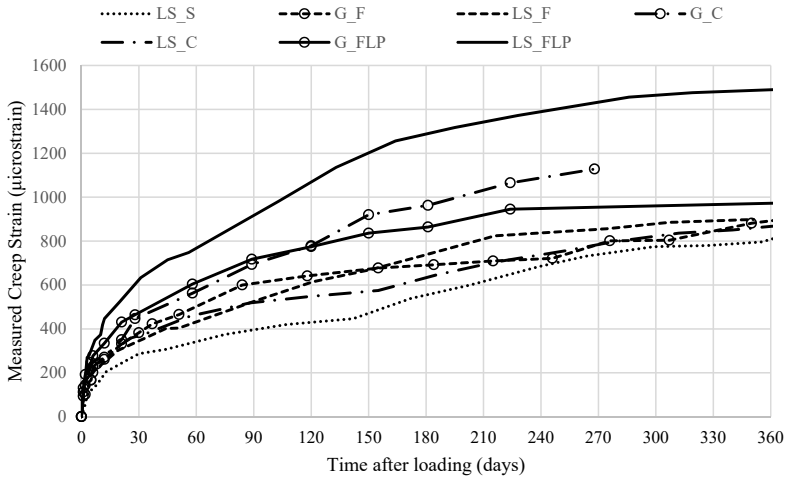

Figure 5. Measured creep strain versus time after loading for all SCC mixtures.

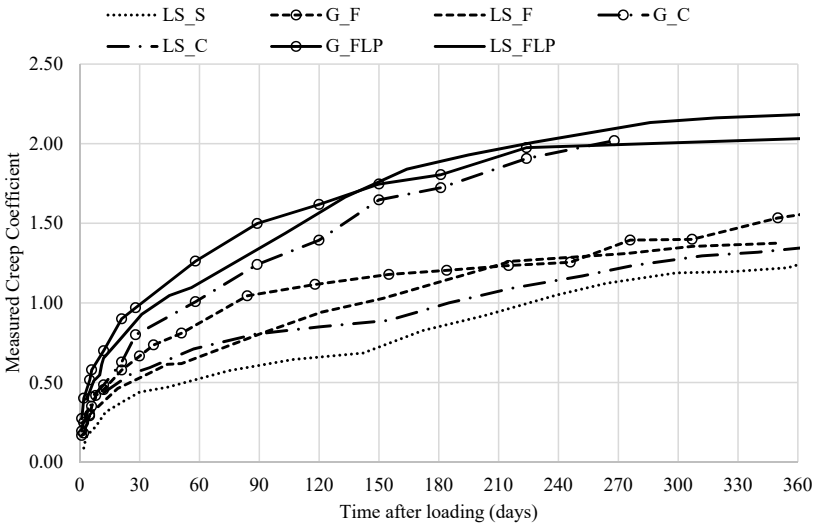

Figure 6. Measured creep coefficient versus time after loading for all SCC mixtures.

Table 8. Statistical analysis results of creep predictions for SCC with different types of SCM/filler.

SCM/Filler Prediction Model	Ratio of Predicted-to-Measured Creep Coefficient													
	F			S			C			FLP			All Mixtures	
	Number of Data Points	Average	Variance	Number of Data Points	Average	Variance	Number of Data Points	Average	Variance	Number of Data Points	Average	Variance	Average	Variance
AASHTO LRFD	38	0.87	0.08	19	0.98	0.02	34	0.78	0.09	33	0.69	0.07	0.82	0.07
ACI 209	38	0.98	0.02	19	1.49	0.15	34	0.98	0.04	33	0.69	0.01	0.97	0.09
CEB-FIP MC90-99	38	2.38	0.75	19	2.09	0.87	34	1.80	0.67	33	1.82	0.14	2.05	0.54
B3	38	1.76	0.11	19	1.83	0.47	34	2.18	0.17	33	1.44	0.17	1.71	0.24
GL2000	38	2.19	0.08	19	3.24	1.47	34	2.18	0.21	33	1.55	0.02	2.15	0.50

Figure 7 also plots the measured and predicted creep coefficient using different models regardless of the type of SCM/filler. The slope of the line of best fit for data points presents the level of prediction accuracy of each model (slope of 1.0 is the highest accuracy). The coefficient of determination, R^2, represents the goodness of fit (the higher R^2, the lower the scatter of the model predictions). This figure indicates that AASHTO LRFD model has the lowest scatter in its predictions, while the GL2000 model has the highest. Table 8 also indicates that in model prediction models, the type of SCM/filler does not have a significant effect on creep coefficient with the exception of mixtures with limestone powder (FLP) that induce higher creep strains, which is in agreement with Heirman [10]. Therefore, it is recommended to use a modification factor greater than 1.0 to adjust creep coefficient prediction for SCC mixtures with limestone powder. The value of this modification factor varies depending on the model used (e.g., 1.2 for AASHTO LRFD model).

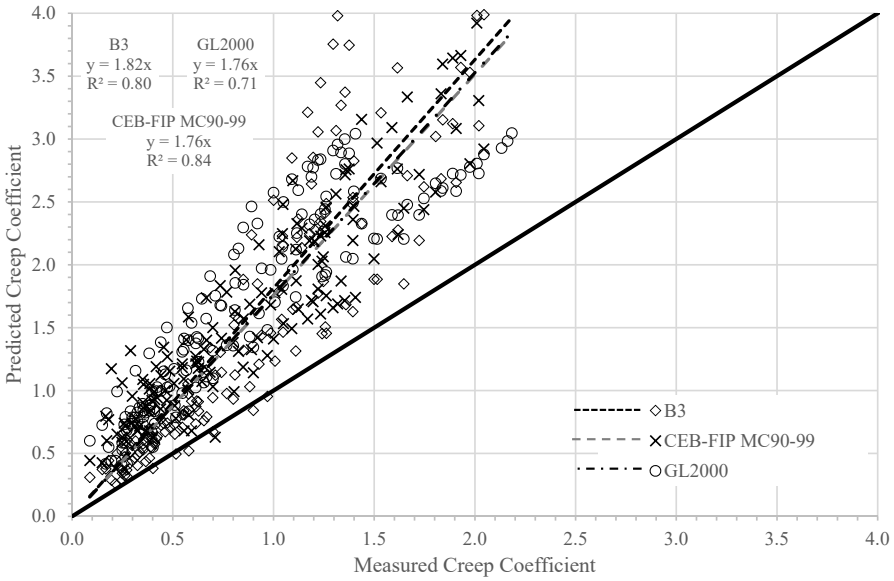

(**a**) B3, CEB-FIP MC90-99, and GL2000

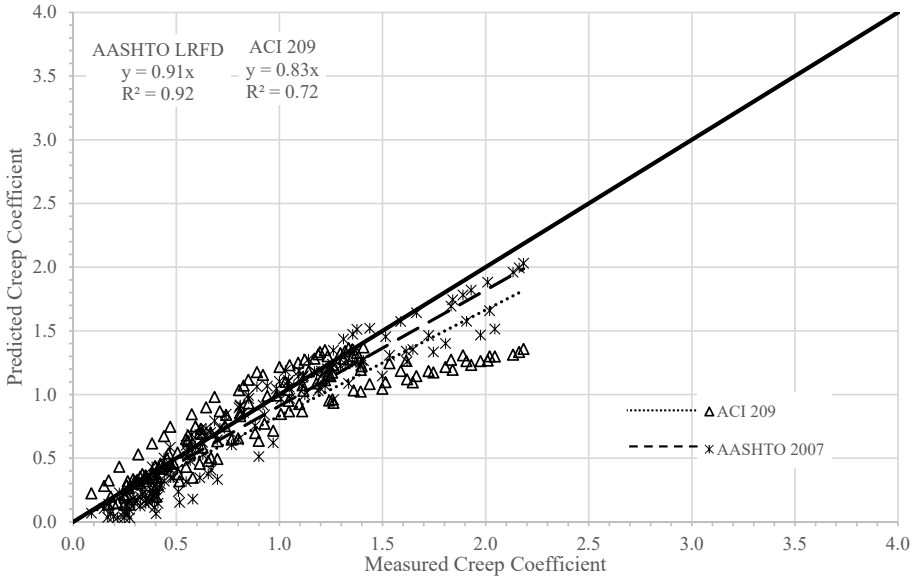

(**b**) ACI 209 and AASHTO LRFD

Figure 7. Comparison of measured and predicted creep coefficient by using different models for all mixtures with different types of SCM/filler.

3.3. Drying Shrinkage Strains

Tables 9 and 10 list the results of measured drying shrinkage at different ages in addition to the average compressive strength at 56 days for mixtures with limestone and gravel aggregate, respectively. Compressive strength at different ages was predicted using the ACI 209 equation if the model does not provide a prediction equation. A graphical presentation of the drying shrinkage strains for all 40 mixtures can be found in the Appendices of NCHRP Report 819 [25].

Table 9. Measured drying shrinkage of SCC mixtures containing limestone aggregate (25 mm = 1 in.; 1 kg/cm^2 = 14.2 psi).

Limestone Mixtures		Measured Drying Shrinkage (μ-Strain)					Compressive Strength (kg/cm^2)
ID	NMAS	3 Day	7 Day	14 Day	28 Day	56 Day	
LS_F_19_LF	19 mm	215	265	365	410	480	45
LS_F_19_HF	19 mm	150	225	340	430	460	45
LS_F_12.5_LF	12.5 mm	35	140	255	420	525	52
LS_F_12.5_HF	12.5 mm	270	260	345	400	435	49
LS_F_9.5_HF	9.5 mm	170	270	365	490	555	48
LS_FLP_19_LF	19 mm	155	175	410	425	470	39
LS_FLP_19_HF	19 mm	55	370	335	450	535	40
LS_FLP_12.5_LF	12.5 mm	80	175	290	380	450	41
LS_FLP_12.5_HF	12.5 mm	150	190	270	360	485	45
LS_FLP_9.5_HF	9.5 mm	130	200	360	410	430	43
LS_S_19_LF	19 mm	120	260	380	460	475	45
LS_S_19_HF	19 mm	135	205	255	310	335	44
LS_S_12.5_LF	12.5 mm	205	375	445	470	570	54
LS_S_12.5_HF	12.5 mm	240	290	330	335	405	55
LS_S_9.5_HF	9.5 mm	200	250	335	470	610	53
LS_C_19_LF	19 mm	160	260	395	495	605	45
LS_C_19_HF	19 mm	125	275	285	345	405	55
LS_C_12.5_LF	12.5 mm	205	300	400	510	680	61
LS_C_12.5_HF	12.5 mm	155	370	410	455	500	56
LS_C_9.5_HF	9.5 mm	245	355	460	640	750	54

Table 10. Measured drying shrinkage of SCC mixtures containing gravel aggregate (25 mm = 1 in.; 1 kg/cm^2 = 14.2 psi).

Gravel Mixtures		Measured Drying Shrinkage (μ-Strain)					Compressive Strength (kg/cm^2)
ID	NMAS	3 Day	7 Day	14 Day	28 Day	56 Day	
G_F_19_LF	19 mm	135	225	360	440	495	32
G_F_19_HF	19 mm	140	275	380	465	525	36
G_F_12.5_LF	12.5 mm	150	255	330	395	505	30
G_F_12.5_HF	12.5 mm	220	270	255	325	475	47
G_F_9.5_HF	9.5 mm	130	320	505	580	660	38
G_FLP_19_LF	19 mm	75	220	340	420	535	40
G_FLP_19_HF	19 mm	105	290	435	555	605	33
G_FLP_12.5_LF	12.5 mm	50	155	345	425	585	33
G_FLP_12.5_HF	12.5 mm	160	255	370	455	605	40
G_FLP_9.5_HF	9.5 mm	150	375	515.3	626	725	32
G_S_19_LF	19 mm	210	355	365	470	540	37
G_S_19_HF	19 mm	165	315	390	430	470	36
G_S_12.5_LF	12.5 mm	170	240	335	425	560	34
G_S_12.5_HF	12.5 mm	140	220	350	405	490	53
G_S_9.5_HF	9.5 mm	175	395	515	590	685	39
G_C_19_LF	19 mm	205	300	405	445	610	40
G_C_19_HF	19 mm	170	270	445	510	610	39
G_C_12.5_LF	12.5 mm	225	350	515	625	760	32
G_C_12.5_HF	12.5 mm	240	260	440	510	670	47
G_C_9.5_HF	9.5 mm	105	385	565	640	735	43

LS = crushed limestone G = gravel F = class F fly ash C = class C fly ash S = GGBFS; FLP = class F fly ash plus limestone powder HF = high flow LF = low flow.

Figure 8 shows that all models underestimate the drying shrinkage; however, GL2000 model provides the closest prediction to measured values, which is in agreement with Mokarem [18]. This model shows higher scatter, as evident in the low R^2 value, compared to the other models as reported by Khayat and Mitchell [15]. The B3 model has the lowest prediction accuracy, which is attributed to low sensitivity to compressive strength. Table 11 shows the statistical data for predicted-to-measured drying shrinkage ratios of SCC mixtures with different types of SCM/filler using each of the five prediction models. It indicates that CEB-FIP MC90-99 and GL2000 models do not have a significant difference in shrinkage prediction, and AASHTO LRFD, ACI 209 and B3 models provide approximately similar drying shrinkage predictions.

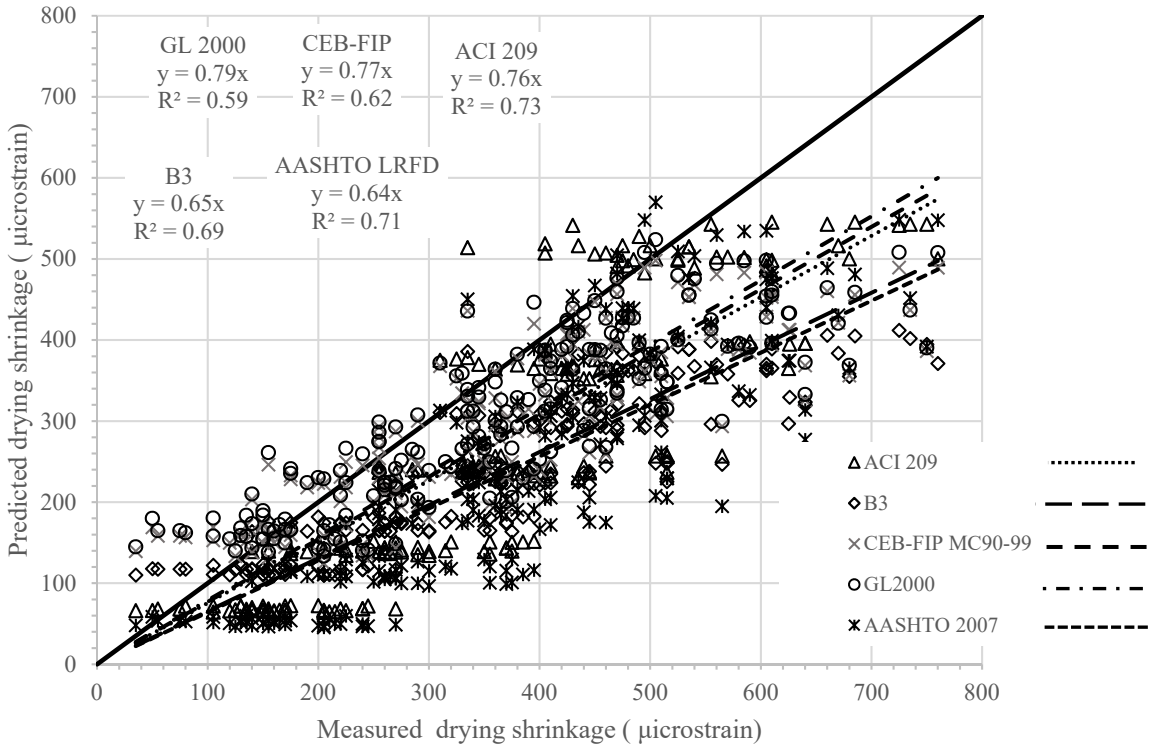

Figure 8. Comparison of measured and predicted drying shrinkage of SCC mixtures using different models.

Table 11. Statistical analysis results of drying shrinkage predictions for SCC containing different types of SCM/filler.

SCM/Filler Prediction Model	Ratio of Predicted-to-Measured Drying Shrinkage Strain													
	F			FLP			S			C			All Mixtures	
	Number of Data Points	Average	Variance	Number of Data Points	Average	Variance	Number of Data Points	Average	Variance	Number of Data Points	Average	Variance	Average	Variance
AASHTO LRFD	50	0.63	0.07	50	0.68	0.05	50	0.58	0.06	50	0.48	0.03	0.59	0.06
ACI 209	50	0.75	0.08	50	0.77	0.05	50	0.71	0.08	50	0.60	0.04	0.71	0.07
GL2000	50	0.99	0.24	50	1.09	0.30	50	0.89	0.05	50	0.74	0.03	0.93	0.17
CEB-FIP MC90-99	50	0.96	0.22	50	1.08	0.27	50	0.84	0.03	50	0.72	0.03	0.90	0.15
B3	50	0.76	0.13	50	0.82	0.13	50	0.69	0.02	50	0.60	0.02	0.72	0.06

4. Conclusions

Evaluation of creep and drying shrinkage prediction models for SCC was conducted using forty SCC mixtures containing different types of coarse aggregate, NMSA, levels of filling ability and types of SCM/filler. Five prediction models were compared using measured data and the following conclusions were made:

1. The AASHTO LRFD model provided better prediction for creep coefficient of SCC with lower scattering of data when different types of SCM/filler were used. On the other hand, using limestone powder increased measured creep strains more than predicted and required the use of a modification factor (greater than 1.0) in all models.
2. The AASHTO LRFD and ACI 209 models provided similar predictions of creep coefficient for SCC, while CEB-FIP MC90-99, B3 and GL2000 models overestimated the creep coefficient significantly.
3. Regardless of the type of SCM/filler, CEB-FIP MC90-99 and GL2000 models provided similar prediction of creep coefficient and drying shrinkage of SCC.
4. All models provided lower prediction of drying shrinkage of SCC. However, GL2000, CEB-FIP MC90-99, and ACI 209 models provided better prediction than AASHTO LRFD and B3 models.
5. Modification factors were needed for all drying shrinkage prediction models to account for the higher drying shrinkage of SCC mixtures. The values of these factors depend on the type of SCM/filler used.

Author Contributions: Conceptualization, M.A. and G.M.; methodology, M.A. and G.M.; validation, M.A. and G.M.; formal analysis, M.A.; investigation, M.A. and G.M.; resources, G.M.; data curation, M.A.; writing—original draft preparation, M.A.; writing—review and editing, G.M.; supervision, G.M.; project administration, G.M.; funding acquisition, G.M. All authors have read and agreed to the published version of the manuscript.

Funding: This research was partially funded by National Cooperative Highway Research Program (NCHRP), Project Number 18-16.

Institutional Review Board Statement: Not applicable.

Informed Consent Statement: Not applicable.

Data Availability Statement: Data can be found in the Appendices of the NCHRP Report 819. http://www.trb.org/NCHRP/Blurbs/174472.aspx (accessed on 3 August 2021).

Acknowledgments: The authors would like to acknowledge the financial support of National Cooperative Highway Research Program (NCHRP) for the NCHRP 18-16 Project. The research was conducted in collaboration with K. Wang, P. Taylor, and Xuhao Wang at Iowa State University (ISU).

Conflicts of Interest: The authors declare no conflict of interest.

Notations

$C_d(t, t_o, t_c)$	Compliance function for drying creep at concrete age t when loading and drying starts at ages t_o and t_c, respectively, B3 model
$C_o(t, t_o)$	Compliance function for basic creep at concrete age t when loading starts at age t_o, B3 model
E_{cmto}	Mean modulus of elasticity of concrete when loading starts at age t_o, psi
$d = 4V/S$	Average thickness of a member, in., ACI 209R-92 model
f	Member shape and size constant, days, ACI 209R-92 model
h	Relative humidity expressed as a decimal
k_c	Factor for the effect of the volume-to-surface ratio, AASHTO 2007
k_f	Factor for the effect of concrete strength, AASHTO 2007

k_h, $\beta(h)$	Correction term for effect of humidity on shrinkage according to B3 and GL2000 models, respectively
k_{hc}	Humidity factor for creep, AASHTO 2007
k_{hs}	Humidity factor for shrinkage, AASHTO 2007
k_s	Factor for the effect of the volume-to-surface ratio, AASHTO 2007
k_{td}	Time development factor, AASHTO 2007
k_{vs}	Factor for the effect of the volume-to-surface ratio of the component, AASHTO 2007
q_1	Inverse of asymptotic elastic modulus, 1/psi, B3 model
$S(t-t_c)$, $\beta_s(t-t_c)$ or $\beta(t-t_c)$	Correction term for effect of time on shrinkage according to B3, CEB MC90, or GL2000 models, respectively
t	Age of concrete, days
$t-t_c$	Duration of drying
t_c	Age of concrete when drying starts at end of moist curing, days
t_o	Age of concrete at loading, days
V/S	Volume-surface ratio, in.
α	Member shape and size constant, 1.0, ACI 209R-92 model
$\beta_c(t-t_o)$	Correction term for effect of time on creep coefficient according to CEB MC90 and CEB MC90-99 models
ε_{cso}	Notional shrinkage coefficient, in./in., CEB MC90 model
ε_{shu} or $\varepsilon_{sh\infty}$	Notional ultimate shrinkage strain, in./in., ACI 209R-92 and GL2000 models and B3 model, respectively
Ψ	Ratio of fine aggregate to total aggregate by weight expressed as percentage, ACI 209R-92 model
ϕ_o	Notional creep coefficient (dimensionless), CEB MC90-99 and GL2000 models
ϕ_u	Ultimate (in time) creep coefficient, ACI 209R-92 model
$\Phi(t_c)$	The correction term for the effect of drying before loading, 1.0, GL2000 model

References

1. ACI Committee 237. *Self-Consolidating Concrete*; American Concrete Institute: Farmington, MI, USA, 2007; p. 29.
2. AASHTO. *AASHTO LRFD Bridge Design Specifications*, 7th ed.; American Association of Highway and Transportation Officials: Washington, DC, USA, 2014.
3. ACI Committee 209. *Prediction of Creep, Shrinkage, and Temperature Effects in Concrete Structure*; American Concrete Institute: Farmington, MI, USA, 1997; p. 47.
4. ACI Committee 209. *Guide for Modeling and Calculating Shrinkage and Creep in Hardened Concrete*; American Concrete Institute: Farmington, MI, USA, 2008; p. 45.
5. CEB-FIP. *Structural Concrete-Textbook on Behavior, Design and Performance Updated Knowledge of the CEB/FIP Model Code 1990*; Federation International du Béton: Lausanne, Switzerland, 1999; pp. 37–52.
6. Bažant, Z.P.; Baweja, S. *Creep and Shrinkage Prediction Model for Analysis and Design of Concrete Structures: Model B3. Adam Neville Symposium: Creep and Shrinkage-Structural Design Effects, ACI SP–194*; Al-Manaseer, A., Ed.; American Concrete Institute: Farmington Hills, MI, USA, 2000; pp. 1–83.
7. Gardner, N.J.; Lockman, M.J. Design Provisions for Drying Shrinkage and Creep of Normal-Strength Concrete. *ACI Mater. J.* **2001**, *98*, 159–167.
8. Leemann, A.; Lura, P.; Loser, R. Shrinkage and Creep of SCC—The Influence of Paste Volume and Binder Composition. *Construct. Build. Mater.* **2011**, *25*, 2283–2289. [CrossRef]
9. Turcry, P.; Loukili, A.; Haidar, K.; Pijaudier-Cabot, G.; Belarbi, A. Cracking Tendency of Self-Compacting Concrete Subjected to Restrained Shrinkage. Experimental Study and Modeling. *J. Mater. Civ. Eng.* **2006**, *18*, 46–54. [CrossRef]
10. Heirman, G.; Vandewalle, L.; Van Gemert, D.; Boel, V.; Audenaert, K.; De Schutter, G.; Desmet, B.; Vantomme, J. Time-dependent deformations of Limestone Powder Type Self-Compacting Concrete. *Eng. Struct.* **2008**, *30*, 2945–2956. [CrossRef]
11. Kavanaugh, B.P. Creep Behavior of Self-Consolidating Concrete. Master's Thesis, Auburn University, Auburn, AL, USA, 2008; p. 209.
12. Kim, Y.H.; Trejo, D.; Hueste, M.B.D.; Kim, J.J. Experimental Study on Creep and Durability of High-Early-Strength Self-Consolidating Concrete for Precast Elements. *ACI Mater. J.* **2011**, *108*, 128–138.
13. AASHTO. *AASHTO LRFD Bridge Design Specifications*, 4th ed.; American Association of Highway and Transportation Officials: Washington, DC, USA, 2007.
14. AASHTO. *AASHTO LRFD Bridge Design Specifications*, 3rd ed.; American Association of Highway and Transportation Officials: Washington, DC, USA, 2004.

15. Khayat, K.H.; Mitchell, D. *Self-Consolidating Concrete for Precast, Prestressed Concrete Bridge Elements*; National Corporative Highway Research Program (NCHRP), Report 628; Transportation Research Board: Washington, DC, USA, 2009.
16. Landsberger, G.A.; Fernandez-Gomez, J. Evaluation of Creep Prediction Models for Self-Consolidating Concrete. In Proceedings of the 5th International RILEM Symposium on Self-Compacting Concrete, Ghent, Belgium, 3–5 September 2007; pp. 605–610.
17. Naito, C.J.; Parent, G.; Brunn, G. Performance of bulb-tee girders made with self-consolidating concrete. *PCI J.* **2006**, *51*, 72–85. [CrossRef]
18. Mokarem, D.W. Development of Concrete Shrinkage Performance specifications. Ph.D. Dissertation, Civil and Environmental Engineering, Virginia Polytechnic Institute, State University, Blacksburg, VA, USA, 2002; p. 225.
19. Vikan, H.; Hammer, T.A.; Kjellsen, O. Drying Shrinkage of SCC—Influence of the Composition of Ternary Composite Cements. In *Proceedings of the 6th International RILEM Symposium on Self-Compacting Concrete, Montreal, Canada*; Springer: Dordrecht, The Netherlands, 2010; pp. 271–282.
20. Gesoğlu, M.; Güneyisi, E.; Özbay, E. Properties of self-compacting concretes made with binary, ternary, and quaternary cementitious blends of fly ash, blast furnace slag, and silica fume. *Construct. Build. Mater.* **2009**, *23*, 1847–1854. [CrossRef]
21. Güneyisi, E.; Gesoğlu, M.; Özbay, E. Strength and drying shrinkage properties of self-compacting concretes incorporating multi-system blended mineral admixtures. *Construct. Build. Mater.* **2010**, *24*, 1878–1887. [CrossRef]
22. Schindler, A.K.; Barnes, R.W.; Roberts, J.B.; Rodriguez, S. Properties of Self-Consolidating Concrete for Prestressed Members. *ACI Mater. J.* **2007**, *104*, 53–61.
23. Lange, D.A.; Struble, L.J.; Dambrosia, M.D.; Shen, L.; Tejeda-Dominguez, F.; Birch, B.F.; Brinks, A.J. *Performance and Acceptance of Self—Consolidating Concrete*; Report FHWA-ICT-08-020; Illinois Center for Transportation: Rantoul, IL, USA, 2008.
24. Hu, J.; Wang, K. Effect of Coarse Aggregate Characteristics on Concrete Rheology. *Elsevier J. Construct. Build. Mater.* **2011**, *25*, 1196–1204. [CrossRef]
25. Morcous, G.; Wang, K.; Taylor, P.C.; Shah, S. *Self-Consolidating Concrete for Cast-in-Place Bridge Components*; National Corporative Highway Research Program (NCHRP), Report 819; Transportation Research Board: Washington, DC, USA, 2016.